ACS APPLIED NANO MATERIALS

www.acsanm.org Article

Enhancing Necroptotic Chemo-Immunotherapy of Breast Cancer by Reactive Oxygen Species Generating Lipid Nanoparticles

Wanting Yang,[#] Ziyao Zhang,[#] Jingxia Xu, Zhuyuan Peng, Fangming Zhang, Xinyu Zhao, Guofeng Li, Yen Wei, Lingyun Zhao, Lin Wang,* Xing Wang,* and Wensheng Xie*

Cite This: *ACS Appl. Nano Mater.* 2025, 8, 14470−14480 Read Online

ACCESS | Metrics & More | Article Recommendations | Supporting Information

ABSTRACT: Advanced breast cancer still suffers a low survival rate and incurable outcome, despite the fact that targeted therapy has significantly improved the therapeutic efficacy. Clinical trials have demonstrated that the combination of immunotherapy and chemotherapy via inducing immunogenicity of tumor cell death during chemotherapy could make a difference. Thus, in this study, both bimetallic FePd nanoparticles (NPs) and 6-diazo-5-oxo-L-norleucine (DON) coloaded reactive oxygen species (ROS)-generating lipid nanoparticles (Lip@FePd-DON NPs) were prepared via the classical thin-film hydration method to enhance necroptotic chemo-immunotherapy for breast cancer treatment. Upon internalization by tumor cells, the Fenton-like performance of bimetallic FePd NPs catalyze intracellular H_2O_2 into toxic ROS. Then, the combination of DON and ROS could effectively induce cell necroptosis via the RIPK3/MLKL pathway. The immunogenicity of necroptotic cell death releases damage-associated molecular patterns, which act as in situ neoantigens to trigger DC maturation and T cell activation, resulting in an efficient immune response with upregulated expression of inflammatory cytokines (TNF-α, IFN-γ, and IL-6). *In vivo* antitumor evaluation based on tumor-bearing mice displayed highly efficient tumor growth inhibition via enhancing necroptotic chemo-immunotherapy. Considering the *in vivo* biocompatibility, this study demonstrated ROS-generating lipid nanoparticles as potential carriers to deliver DON for enhancing necroptotic chemo-immunotherapy of breast cancer, which may promote the development of personalized nanoplatforms for breast cancer treatment.

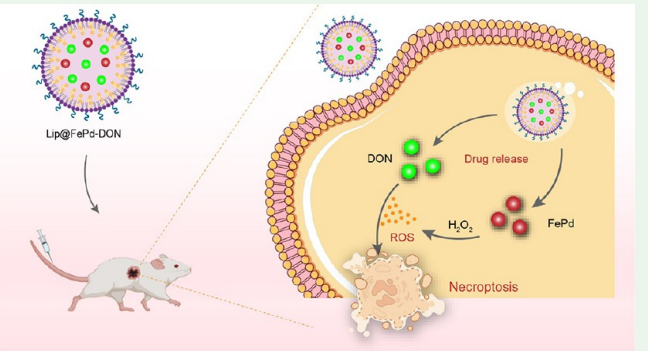

KEYWORDS: *chemo-immunotherapy, necroptosis, reactive oxygen species, 6-diazo-5-oxo-L-norleucine, breast cancer*

1. INTRODUCTION

As one of the most common cancers among women worldwide, breast cancer still suffers a low 5 year survival rate of only 20% with a median overall survival of 2−3 years.[1] Although the development of anticancer agents, including cyclin-dependent kinase 4/6 inhibitors and antibody-drug conjugates, has significantly improved the therapeutic outcome of patients,[2,3] the incurable situation requires new therapeutic options and multidisciplinary treatments to alleviate symptoms, improve quality of life, and prolong patients' survival.[4,5] A recent study has demonstrated that the combination of cancer immunotherapy with chemotherapy achieved effective results in both advanced and early setting phase 3 clinical trials for triple-negative breast cancer.[6] These results encourage researchers to investigate combining immunotherapies, especially the innate immune response, to overcome the challenge of breast cancer treatment. One of the gold standard strategies to induce the immunogenicity of tumor cell death is to employ dead or dying cells as an in situ tumor vaccine to immunize the syngeneic body.[7,8] However, traditional drugs for breast cancer chemotherapy tend to induce cell apoptosis, which is weakly immunogenic and therefore not enough to trigger an efficient immune response.

Necroptosis, an inflammatory form of cell death, has been demonstrated to effectively trigger the release of damage-associated molecular patterns (DAMPs) (such as ATP, CRT, and HMGB1) for host antitumor immune response.[9] More importantly, necroptosis is the first alternative pathway of cell death when the apoptosis is blocked.[10] Therefore, compared with classical chemotherapeutic apoptosis, the design of nanomedicine to induce tumor cell necroptosis may make breakthroughs in therapeutic outcomes for breast cancer by enhanced chemo-immunotherapy. 6-Diazo-5-oxo-L-norleucine (DON), a broadly active glutamine antagonist that suppresses cancer metabolism, has exhibited remarkable antitumor

Received: June 23, 2025
Revised: June 30, 2025
Accepted: July 1, 2025
Published: July 7, 2025

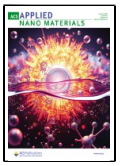

https://doi.org/10.1021/acsanm.5c02985
ACS Appl. Nano Mater. 2025, 8, 14470−14480

Scheme 1. Nanozyme-Enhanced Tumor Necroptosis to Trigger Immune Response by Lip@FePd-DON NPs[a]

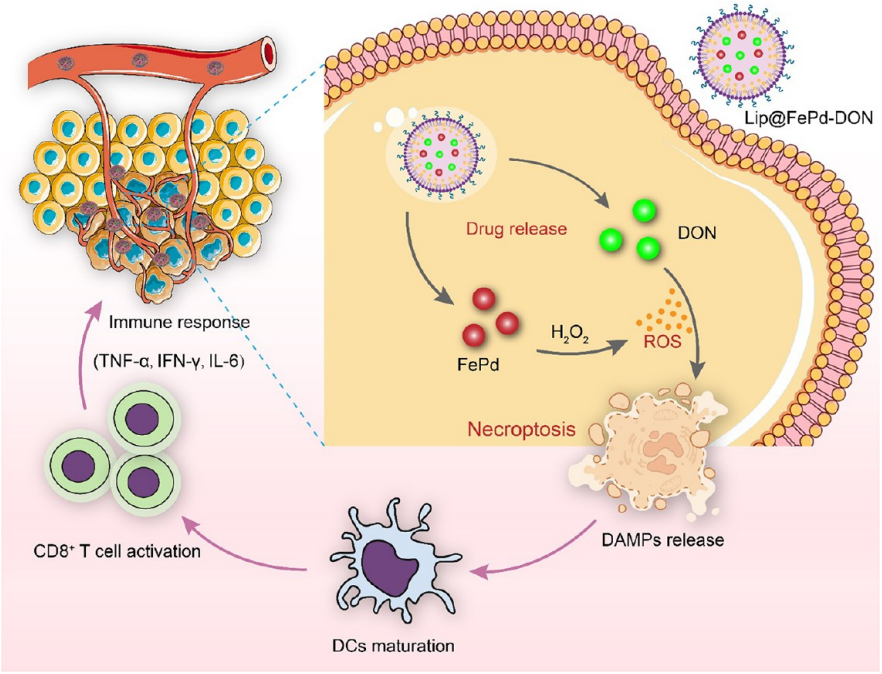

[a]Once endocytosed by tumor cells during blood circulation, Lip@FePd-DON NPs will degrade to release FePd nanozymes and DON. Then, the biocatalysis property of FePd nanozymes transfers intracellular H_2O_2 into ROS to sensitize the cell necroptosis triggered by DON. Subsequently, the immunogenic cell death resulting from necroptosis releases DAMPs as in situ neoantigens to mature DCs and activate $CD8^+$ T cells, leading to an immune response.

efficacy in clinical trials.[11,12] However, its further application was greatly halted by dose-limiting gastrointestinal toxicities to normal tissues.[13] To address this challenge, DON-based prodrug strategies have been widely designed to selectively deliver DON to tumor tissues while blocking cytotoxicity to normal glutamine-dependent tissues.[14−16] Furthermore, effective drug delivery systems were constructed for stability protection, targeted delivery, and decreased cytotoxicity.

Lipid nanoparticles have emerged as the most successful vehicles across the pharmaceutical industry to deliver a variety of therapeutics.[17] Thus, in this study, ROS-generating lipid nanoparticles were constructed via loading bimetallic FePd nanoparticles (NPs) to deliver DON (namely Lip@FePd-DON NPs) for enhancing necroptotic chemo-immunotherapy of breast cancer. Lipid nanoparticle encapsulation guarantees the stability of DON and increases the accumulation of Lip@FePd-DON NPs in tumor tissues during blood circulation (Scheme 1). Once uptake by cells, both bimetallic FePd NPs and DON are released from lipid nanoparticles via lysosome dissociation. The biocatalytic performance of bimetallic FePd NPs catalyzes intracellular H_2O_2 into toxic reactive oxygen species (ROS). Meanwhile, the combination of DON and ROS could effectively induce cell necroptosis via the RIPK3/MLKL pathway. Then, the release of DAMPs by immunogenic necroptotic tumor cells will act as in situ neoantigens to trigger DCs maturation and T cell activation, resulting in an efficient immune response with expression of inflammatory cytokines (TNF-α, IFN-γ, and IL-6). Considering the effective *in vivo* antitumor efficacy, this study demonstrated ROS-generating lipid nanoparticles as potential carriers to deliver DON for enhancing necroptotic chemo-immunotherapy of breast cancer.

2. MATERIALS AND METHODS

2.1. Chemical Materials. Palladium acetylacetonate, iron acetylacetonate, poly(vinylpyrrolidone) (PVP, Mw = 30k), cetyltrimethylammonium bromide (CTAB) 1,2-dipalmitoyl-*sn*-glycero-3-phosphocholine (DPPC), 1,2-distearoyl-*sn*-glycero-3-phosphoethanolamine-poly(ethylene glycol) (DSPE-PEG), and cholesterol were brought from Sigma-Aldrich LLC. Relevant cell assay kits were purchased from Solarbio Life Sciences & Technology Co., Ltd., including CCK-8, DCFH-DA, calcein-AM, PI, and Hoechst33342. ELISA assay kits (TNF-α, IFN-γ, IL-6) were brought from Beyotime Biotechnology Co., Ltd. 6-Diazo-5-oxo-L-norleucine (DON) was purchased from Zancheng (Tianjin) Technology LLC. Anti-RIPK3 primary antibody, anti-GAPDH primary antibody, and secondary antibody were obtained from Cell Signaling Technology, Inc. All chemicals were used without any purification.

2.2. Synthesis of Lip@FePd-DON NPs. First, the FePd nanozymes were prepared and guided by our previous study.[18] Lip@FePd-DON NPs were synthesized by following a standard thin-film hydration method. Generally, cholesterol, DPPC, and DSPE-PEG were completely dissolved in 20 mL of chloroform (67:30:3 mol ratio). Then, the solvent was evaporated by rotary evaporation in a round-bottom flask to form a thin film of lipids. Four mL of PBS containing 8 mg of FePd nanozymes and 80 μg of DON was added to dissolve the film. The mixture was hydrated by gentle vortex and sonication (300 W, 2 min) under an ice bath. The final Lip@FePd-DON NPs were obtained and purified via centrifugation.

2.3. Characterization. The morphology of as-synthesized nanoparticles was measured by a transmission electron microscope (TEM, Hitachi). The size distribution and zeta potential were measured by dynamic light scattering (DLS, Malvern). UV−vis−NIR absorption was obtained by a microplate reader (Thermal). All confocal fluorescence images were evaluated by a confocal laser scanning microscope (CLSM, Zeiss).

2.4. Biocatalytic Performance and Kinetics Evaluation. The biocatalytic ability of Lip@FePd-DON NPs to transfer H_2O_2 into ROS was tested via a colorimetric method (TMB single-component

https://doi.org/10.1021/acsanm.5c02985
ACS Appl. Nano Mater. 2025, 8, 14470−14480

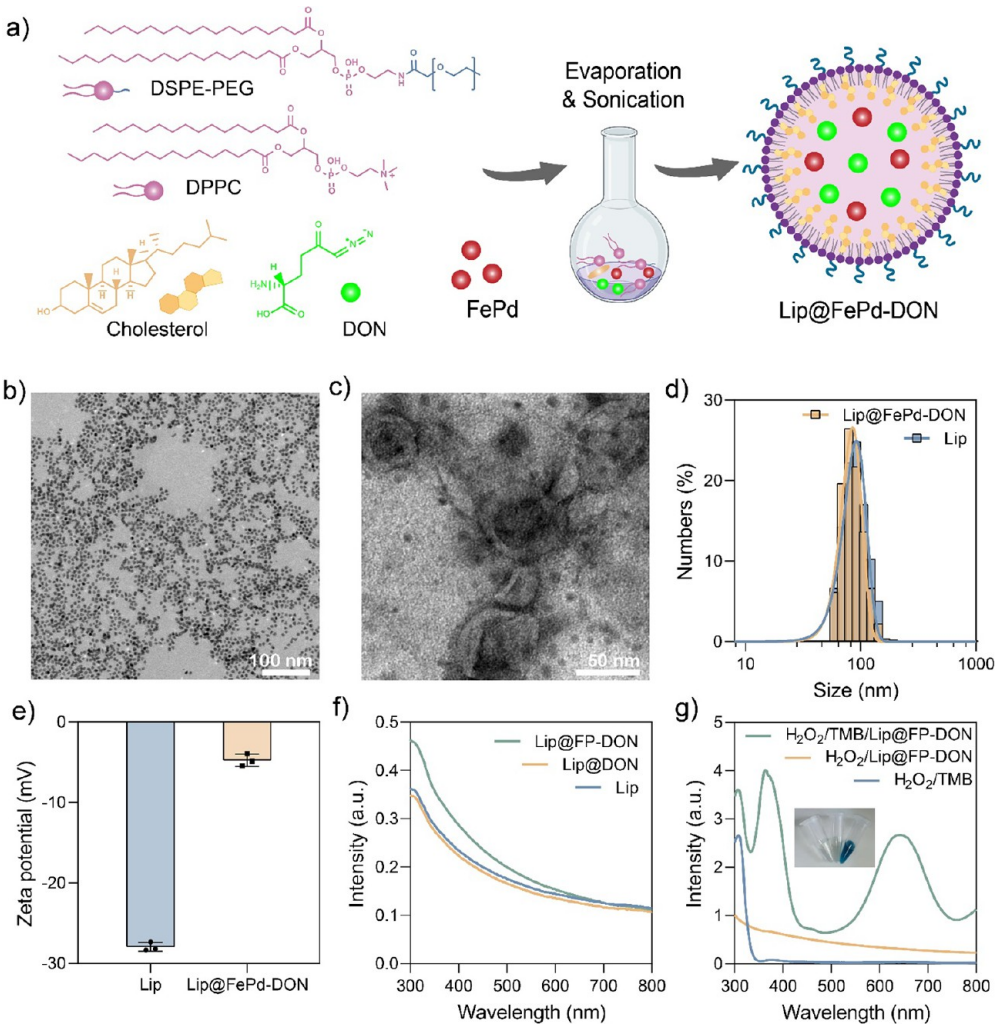

Figure 1. Preparation and characterization of Lip@FePd-DON NPs. (a) Schematic illustration of preparing both DON and FePd codelivered Lip@FePd-DON NPs via the thin-film hydration strategy. (b) TEM images of FePd NPs in aqueous solution. (c) TEM images of as-synthesized Lip@FePd-DON NPs. (d) Size distribution of Lip and Lip@FePd-DON NPs measured by DLS. (e) Zeta potential of Lip and Lip@FePd-DON NPs in aqueous solution. (f) UV−vis−NIR absorption curve of Lip, Lip@DON, and Lip@FePd-DON aqueous solutions (100 μg/mL). (g) UV−vis−NIR absorption curve of H_2O_2/TMB, H_2O_2/Lip@FePd-DON, and H_2O_2/TMB/Lip@FePd-DON mixture.

substrate solution). Generally, Lip@FePd-DON NPs (100 μg/mL) were mixed with TMB single-component substrate solution and H_2O_2 solution in pH 4.0 buffer under a 37 °C environment. One hour later, UV−vis−NIR absorption spectra were measured by a microplate reader to analyze the typical absorbance at about 652 nm. Meanwhile, the concentration-dependent biocatalytic performance of Lip@FePd-DON NPs (40, 80, 120, 160, and 200 μg/mL) and H_2O_2 substrate (1, 10, 20, 40, and 80 μM) was evaluated in a similar method. To identify the kinetics, the Michaelis−Menten model was employed to test the catalytic efficacy under different $_2O_2$ substrates.

2.5. Intracellular ROS Detection. 4T1 cells were seeded into a confocal dish with a density of 20,000 cells per dish. After adherent growth, fresh media containing different formulations (PBS, Lip, Lip@FePd, Lip@DON, and Lip@FePd-DON NPs) (50 μg/mL) were replaced and coincubated for another 8 h. Cells were washed with PBS and then stained with 2′,7′-dichlorofluorescein diacetate (DCFH-DA) fluorescent probe. Fluorescence images were obtained via CLSM.

2.6. Cell Cytotoxicity Measurement of DON, Lip, and Lip@FePd-DON NPs. 4T1 cells were seeded into a 96-well plate with a density of 5000 per well. After adherent growth, fresh media containing different concentration formulations (DON, Lip, Lip@FePd-DON) were used to replace the old one and coincubated for another 24 h. Then, the relative cell viability was measured by the CCK-8 assay. Meanwhile, calcein-AM was used to stain the live cells for visual evaluation of the cell state. GraphPad Prism software was used to calculate the half-maximal inhibitory concentration (IC50) value.

2.7. Hoechst33342/PI Double Staining for Necroptosis. 4T1 cells were seeded into a confocal dish with a density of 20,000 per dish. After adherent growth, fresh media containing different formulations (PBS, Lip, Lip@FePd, Lip@DON, and Lip@FePd-DON NPs) (62.5 μg/mL) were replaced and coincubated for another 12 h. Cells were washed with PBS and then stained with the Hoechst33342/PI fluorescent probe according to the standard protocol. Fluorescence images were obtained via CLSM.

2.8. Western Blotting Measurement. 4T1 cells were seeded into a Petri dish with a density of 500,000 cells per dish. After adherent growth, fresh media containing different formulations (PBS, Lip, Lip@FePd, Lip@DON, and Lip@FePd-DON NPs) (62.5 μg/mL) were replaced and coincubated for another 12 h. Protein was extracted by RIPA buffer with the protection of phenylmethanesulfonylfluoride. After SDS-PEGE electrophoresis and PVDF membrane transfer, the membrane was incubated with anti-RIPK3 (1:1000) and anti-GAPDH (1:1000) primary antibodies for 12 h under a 4 °C environment. Then, a horseradish-peroxidase-conjugated goat anti-rabbit IgG (1:2000) secondary antibody was used to label the target

https://doi.org/10.1021/acsanm.5c02985
ACS Appl. Nano Mater. 2025, 8, 14470−14480

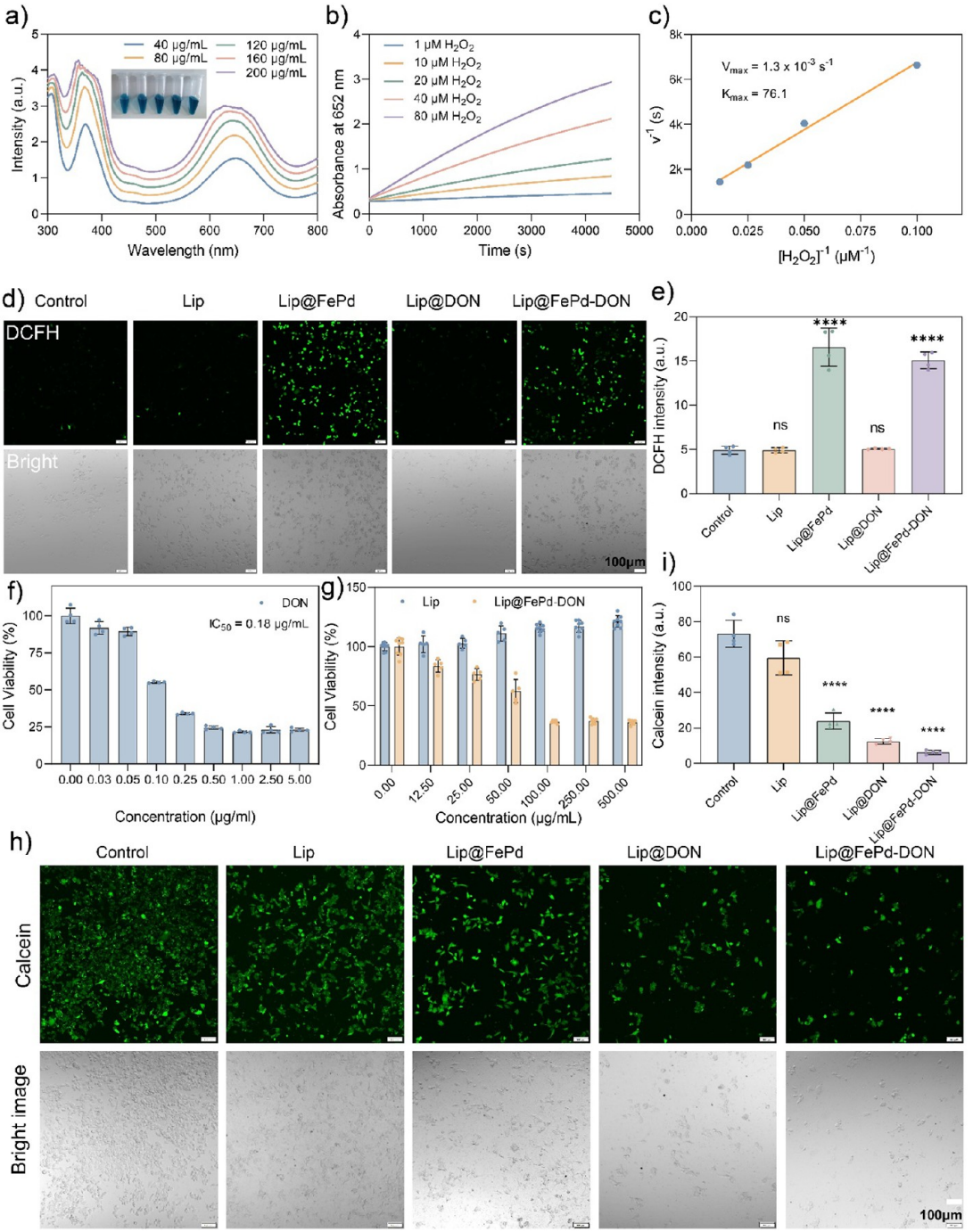

Figure 2. In vitro biocatalytic performance and cytotoxicity of as-prepared Lip@FePd-DON NPs. (a) UV−vis−NIR absorption curve of H_2O_2/TMB/Lip@FePd-DON mixture with various Lip@FePd-DON NPs concentrations (40, 80, 120, 160, and 200 μg/mL). Inset are the corresponding photographs. (b) Time-dependent absorption of H_2O_2/TMB/Lip@FePd-DON mixture with various H_2O_2 concentrations (1, 10, 20, 40, and 80 μM). (c) Michaelis−Menten kinetics and Lip@FePd-DON NPs upon the various concentrations of H_2O_2 (1, 10, 20, 40, and 80 μM). (d, e) Confocal fluorescence images and corresponding average fluorescence intensities of 4T1 cells treated with PBS, Lip, Lip@FePd, Lip@DON, and Lip@FePd-DON NPs (50 μg/mL) for 8 h and then stained with DCFH-DA (intracellular ROS) probe. (f) Cell viability of 4T1 cells treated with various concentrations of DON for 24 h. (g) Cell viability of 4T1 cells treated with various concentrations of Lip and Lip@FePd-DON NPs, respectively. (h, i) Confocal fluorescence images and corresponding average fluorescence intensities of 4T1 cells treated with PBS, Lip, Lip@FePd, Lip@DON, and Lip@FePd-DON NPs (62.5 μg/mL) for 24 h and then stained with calcein-AM (live cells) probe.

protein. Finally, the membrane was visualized by a luminescent imager (ImageQuant LAS 4000).

2.9. Animal Model and *In Vivo* Antitumor Efficacy. Six-week-old female Balb/c mice were purchased from Beijing Vital River Laboratory Animal Technology Co., Ltd. and fed according to the guidelines of the Laboratory Animal Research Center, Tsinghua University (No. 23-LYZ). 4T1 cells were subcutaneously injected to establish the tumor-bearing mouse model. When the tumor volume reached about 100 mm^3, mice were randomly divided into five groups (n = 4): control group intravenously (iv) injected with PBS; Lip@FePd group iv injected with Lip@FePd (10 mg/mL, 100 μL); Lip@DON group iv injected with Lip@DON (10 mg/mL, 100 μL); and

https://doi.org/10.1021/acsanm.5c02985
ACS Appl. Nano Mater. 2025, 8, 14470−14480

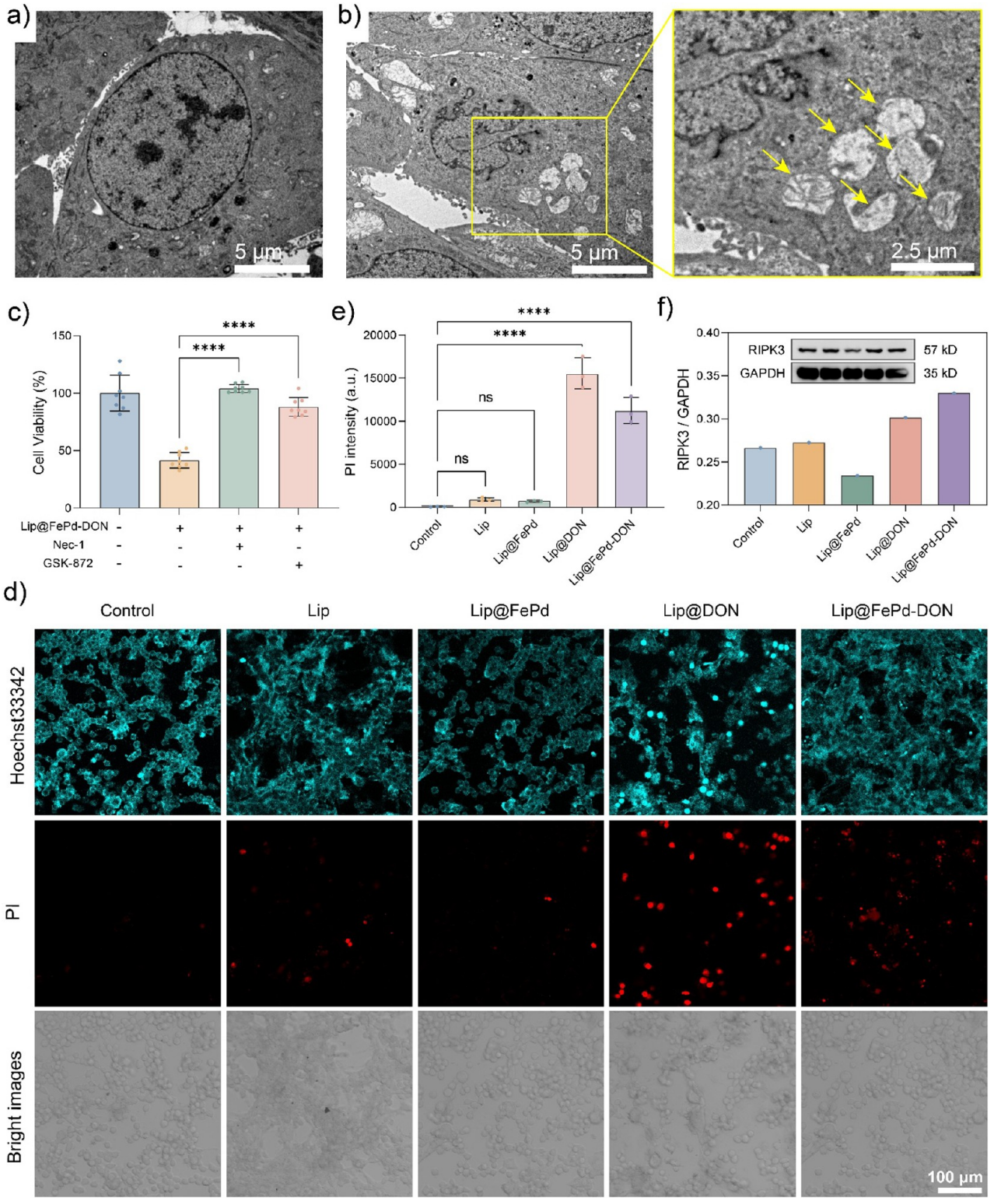

Figure 3. Induced necroptosis of 4T1 cells via Lip@FePd-DON. (a, b) TEM images of 4T1 cell slices after treatment with PBS (a) and Lip@FePd-DON NPs (b) for 12 h. (c) Cell viability of 4T1 cells treated with different formulations (Lip@FePd-DON, Nec-1, and GSK-872). (d, e) Confocal fluorescence images and corresponding average fluorescence intensities of 4T1 cells treated with PBS, Lip, Lip@FePd, Lip@DON, and Lip@FePd-DON NPs (62.5 μg/mL) for 12 h and then stained with Hoechst33342 and PI probe for necroptosis analysis. (f) Western blotting analysis of the expression RIPK3 protein in various treated 4T1 cells.

Lip@FePd-DON group iv injected with Lip@FePd-DON (10 mg/mL, 100 μL). The body weight of mice and tumor volume were recorded every 2 days. Seventeen days later, all mice were sacrificed to extract main organs and tumor tissues for further evaluation.

2.10. Immunohistology and Immunofluorescence Analysis.

All the main organs (heart, liver, spleen, lung, and kidney) and tumor tissues were fixed, embedded, sliced, and stained for immunohistology analysis (H&E) and immunofluorescence analysis (K_i-67 and

https://doi.org/10.1021/acsanm.5c02985
ACS Appl. Nano Mater. 2025, 8, 14470−14480

TUNEL). Meanwhile, the expression level of cytokines (TNF-α, IFN-γ, IL-6) in tumor tissues was measured by the corresponding ELISA kit.

2.11. Statistical Analysis. All data were presented as mean values ± SD, and the statistical difference was calculated by two-tailed student's t test and one-way ANOVA. *$p < 0.05$, **$p < 0.01$, ***$p < 0.001$, and ****$p < 0.0001$.

3. RESULTS AND DISCUSSION

3.1. Synthesis and Characterization of Lip@FePd-DON Nanoparticles. The Lip@FePd-DON NPs were fabricated via classical thin-film hydration with loading bimetallic FePd NPs and DON drug (Figure 1a).[18] 1,2-Dipalmitoyl-*sn*-glycero-3-phosphocholine (DPPC) and 1,2-distearoyl-*sn*-glycero-3-phosphoethanolamine-poly(ethylene glycol) (DSPE-PEG) were chosen as main components of lipid nanoparticles. Meanwhile, the bimetallic FePd NPs were prepared via a carbon monoxide-mediated reduction reaction with palladium acetylacetonate and iron acetylacetonate as precursors. As shown in Figure 1b, as-synthesized FePd NPs exhibited uniform size distribution and well dispersibility in aqueous conditions, which will benefit the encapsulation efficiency in lipid nanoparticles. The TEM images of Lip@FePd-DON NPs (Figure 1c) and pure Lip NPs (Figure S1) displayed the typical double membrane structure with FePd NPs inlaying into the lipid nanostructures. A few FePd NPs were scattered out of the membrane of Lip@FePd-DON NPs due to the good dispersibility in an aqueous solution. The dynamic hydrated particle size of naked Lip NPs was about 91.58 nm with a surface zeta potential of −27.83 mV (Figure 1d&e). However, the size of Lip@FePd-DON NPs slightly decreased to 85.06 nm, and the zeta potential significantly increased to −4.65 mV due to the positive potential of DON (Figure 1e). The UV−vis−NIR spectrum of DON aqueous solution revealed that there was no typical absorption peak between 300 to 800 nm (Figure S2). Therefore, the UV−vis−NIR spectra of both Lip@DON and Lip@FePd-DON were similar to those of Lip (Figure 1f). Our previous study has reported the excellent Fenton-like catalytic performance of as-synthesized FePd NPs which would effectively transfer H_2O_2 substrate into hydroxyl radical.[18] Thus, the catalytic ability of Lip@FePd-DON NPs was systematically evaluated via a colorimetric method to explore the stability of FePd NPs. As shown in Figure 1g, both H_2O_2/TMB and TMB/Lip@FePd-DON mixtures did not present any characteristic absorption peak because of the lack of catalyst and zymolyte, respectively. A typical absorption peak around 652 nm was detected in the H_2O_2/TMB/Lip@FePd-DON mixture, demonstrating the successful generation of abundant ROS. The deep blue color of H_2O_2/TMB/Lip@FePd-DON (Figure 1g) visually exhibited the catalytic performance compared to H_2O_2/TMB and TMB/Lip@FePd-DON. These results confirmed the ROS-generating ability of Lip@FePd-DON.

3.2. Intracellular ROS-Generating Ability and *In Vitro* Cytotoxicity. The catalytic kinetics of Lip@FePd-DON NPs were first evaluated before testing the intracellular ROS-generating ability. As shown in Figure 2a, Lip@FePd-DON exhibited a concentration-dependent catalytic performance. The color of the mixture clearly showed the improved reaction rate with the increase in concentration. Meanwhile, the catalytic efficiency of Lip@FePd-DON increased with the concentration of H_2O_2 substrate increased from 1 to 80 μM (Figure 2b and Figure S3). It is well-known that the concentration of H_2O_2 in tumor cells is about 50−100 μM while the concentration of H_2O_2 in normal cells is 1−100 nM.[19] Therefore, as-synthesized Lip@FePd-DON NPs could ensure the ROS-generating performance in the tumor cell. Furthermore, Michaelis−Menten kinetics was employed to simulate the catalytic process. As shown in Figure 2c, the maximum reaction rate (V_{max}) was about 1.3×10^{-3} per second with a Michaelis constant (K_{max}) of 76.1. Considering the effective catalytic performance, the intracellular ROS-generating ability of Lip@FePd-DON NPs in 4T1 cells was measured using the DCFH-DA fluorescence probe (Figure 2d). Few green fluorescence was detected in the control, Lip, and Lip@DON groups. In contrast, significantly strong green fluorescence appeared in both Lip@FePd and Lip@FePd-DON coincubation groups, indicating the abundant ROS generation catalyzed by the FePd component in both Lip@FePd and Lip@FePd-DON NPs (Figure 2e). These results will guarantee further exploration of the ROS-enhanced cytotoxicity of DON.

The *in vitro* cytotoxicity of free DON to 4T1 cells was tested via the coincubation method. As shown in Figure 2f and Figure S4, DON exhibited high cytotoxicity to 4T1 cells with a low IC50 value of 0.18 μg/mL, which means that DON is one of sensitive chemotherapeutic drugs for breast cancer. Naked Lip carriers demonstrated excellent biocompatibility to 4T1 cells, even with a high concentration of 500 μg/mL (Figure 2g). In contrast, Lip@FePd-DON presented a dose-dependent cytotoxicity trend with an IC50 value of about 66.23 μg/mL. The fluorescence images stained by the calcein-AM probe (Figure 2h) showed abundant live cells in the control and Lip groups after 24 h of coincubation. However, Lip@FePd and Lip@DON treatment resulted in decreased cell viability of about 23.93% and 12.48, respectively (Figure 2h&i), demonstrating the efficient antitumor efficacy of Lip@FePd-mediated ROS generation and Lip@DON-mediated chemotherapy. More importantly, the cell viability of 4T1 after Lip@FePd-DON treatment was only 6.23%, indicating the combined cytotoxicity between intracellular ROS and DON.

3.3. Induced Cell Necroptosis via ROS-Enhanced Chemotherapy. It is well-known that cells present different morphological features when dying and necroptotic cells show ballooning of mitochondria, outer membrane disruption, organelle expulsion, and nuclear chromatin irregularities.[20] Lip@FePd-DON NPs treated 4T1 cells were fixed, sliced, stained, and imaged by TEM. Cells in the Control group (Figure 3a) displayed an intact cellular membrane, nuclear, cytoplasm, and mitochondria. In contrast, cells treated with Lip@FePd-DON NPs (Figure 3b) exhibited irregular nuclear chromatin damage, incomplete plasma membrane, and ballooning mitochondria, which were well matched with the typical characteristics of necroptotic cells. The classic core members of the necrosome during necroptotic death are receptor-interacting protein kinase 1 and 3 (RIPK1, RIPK3) and mixed lineage kinase-like protein (MLKL).[21,22] Therefore, the RIPK1 kinase inhibitor (necrostatin-1, Nec-1) and RIPK3 kinase inhibitor (GSK-872) were employed to verify the necroptotic cell death. As shown in Figure 3c, the cell viability of 4T1 cells treated with Lip@FePd-DON decreased to 41.59% compared with the nontreated cells. The cell viability returned to 100.00% and 88.65% when inhibited by Nec-1 and GSK-872, respectively (Figure 3c), demonstrating that Lip@FePd-DON-induced cell death was regulated by RIPK1 and

https://doi.org/10.1021/acsanm.5c02985
ACS Appl. Nano Mater. 2025, 8, 14470−14480

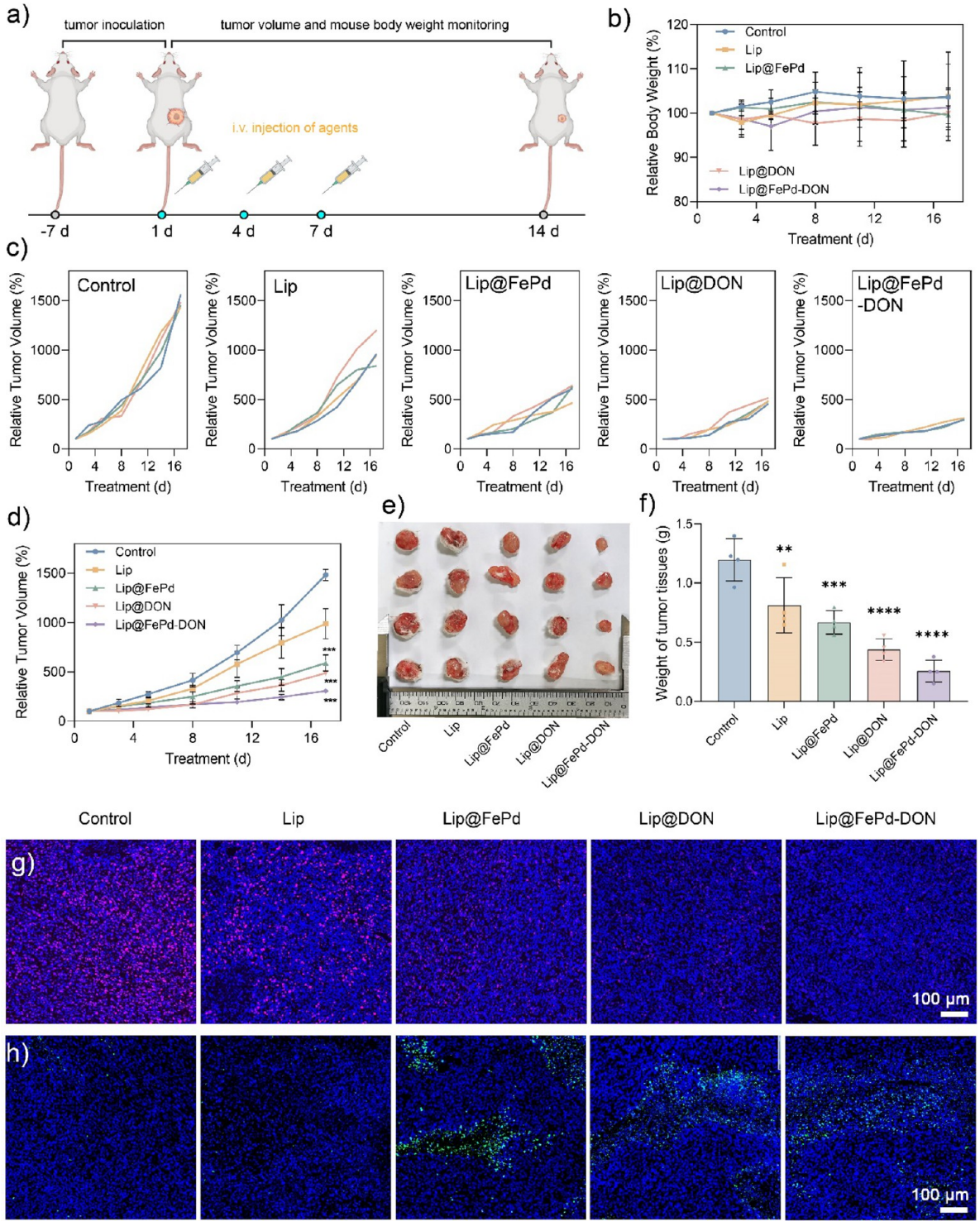

Figure 4. *In vivo* antitumor efficacy of Lip@FePd-DON NPs. (a) Schematic illustration of the *in vivo* antitumor procedures based on 4T1 tumor-bearing mice. Nanoformulations were intravenously (iv) injected on days 1, 4, and 7. (b) Body weight of mice in different groups during 17 days of treatment. (c) Relative tumor volume change of each mouse in different groups (control, Lip, Lip@FePd, Lip@DON, and Lip@FePd-DON). (d) Average tumor volume change of mice in each group (control, Lip, Lip@FePd, Lip@DON, and Lip@FePd-DON) during the treatment. (e, f) Photographs and average weight of tumor tissues in different groups after 17 days of treatment. (g, h) Immunofluorescence images (K_i-67 for g, and UTNEL for h) of tumor tissues with cell nucleus stained with DAPI (blue) after 17 days of treatment.

RIPK3, which were typical characteristics of the necroptotic pathway.[21]

Furthermore, Hoechst 33342/pyridine iodide (PI) double could distinguish the necroptotic cells from the apoptotic ones via membrane integrity. The PI dye could label necrotic cells from normal and apoptotic cells, while Hoechst 33342 dye could label all apoptotic cells from nonapoptotic cells. As shown in Figure 3d,e, a few double Hoechst 33342+/PI+ cells were detected in the control, Lip, and Lip@FePd groups, indicating that alone ROS could not induce cell necroptosis.

https://doi.org/10.1021/acsanm.5c02985
ACS Appl. Nano Mater. 2025, 8, 14470−14480

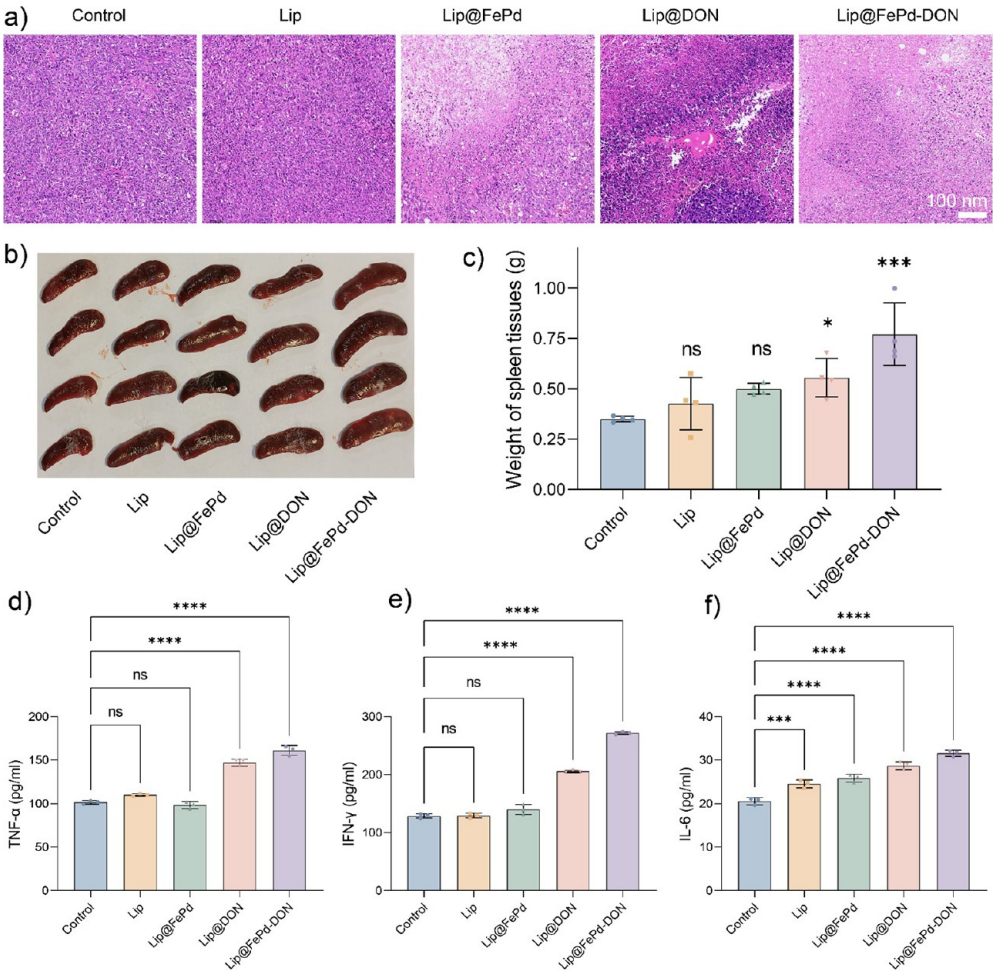

Figure 5. Immune response evaluation of mice after Lip@FePd-DON treatment. (a) Immunohistology images (H&E) of tumor tissues in different groups after 14 days of treatment. (b, c) Photographs and average weight of spleen in different groups after 14 days of treatment. (d–f) ELISA analysis of secretion level of cytokine TNF-α (d), IFN-γ (e), and IL-6 (f) in tumor tissues after 14 days of treatment.

Lip@DON and Lip@FePd-DON-treated cells displayed strong Hoechst 33342+/PI+ signals, directly suggesting the necroptotic state rather than apoptotic ones. To further evaluate the expression of necroptotic protein (RIPK3) after various formulation treatments, western blotting analysis was employed. Compared with the cells in the Control group, Lip and Lip@FePd treated cells exhibited no difference for RIPK3 kinase expression (Figure 3f and Figure S5). However, increased expression of RIPK3 kinase was detected in cells treated by Lip@DON, showing the induced cell necroptosis by Lip@DON NPs. More importantly, Lip@FePd-DON-treated cells presented the highest level of RIPK3 kinase, demonstrating the enhanced cell necroptosis by FePd NPs-combined DON treatment. The above results revealed that as-synthesized Lip@FePd-DON NPs could successfully induce necroptosis of breast cancer via ROS-enhanced chemotherapy of DON.

3.4. *In Vivo* Antitumor Efficacy of Lip@FePd-DON NPs. Based on the effective *in vitro* cytotoxicity, a 4T1 tumor-bearing animal model was established in female BALB/c mice to evaluate the *in vivo* antitumor efficacy of Lip@FePd-DON NPs, while taking Lip, Lip@FePd, and Lip@DON as reference. When the tumor volume reached about 100 mm^3, mice were randomly divided into five groups (n = 4): Control (iv injected with PBS), Lip (iv injected with Lip), Lip@FePd (iv injected with Lip@FePd), Lip@DON (iv injected with Lip@DON), and Lip@FePd-DON (iv injected with Lip@FePd-DON). The administration dose for each formulation was 10 mg/mL and the whole experiment was implemented according to the procedures in Figure 4a. Compared to mice in the control group, the average body weight of mice in the other four groups showed no significant difference (Figure 4b), demonstrating good *in vivo* biocompatibility and biosafety. A rapid growth rate (almost 15-fold) of the tumor in the control group was recorded during the 14 days of treatment (Figure 4c). Lip treatment exhibited slight tumor growth inhibition but no significant difference (Figure 4d). In comparison, Lip@FePd and Lip@DON-treated mice presented an outstanding antitumor efficacy owing to their catalysis-mediated ROS boosting and chemotherapy-mediated necroptosis, respectively (Figure 4c,d). More importantly, mice in the Lip@FePd-DON-treated group displayed the highest tumor growth inhibition, with only a 3-fold size change compared with the original one, demonstrating the efficient antitumor efficacy of ROS boosting enhanced necroptosis.

After 14 days of treatment, the tumor tissues in each group were collected for further immunohistology and immunofluorescence analysis. The photographs (Figure 4e) and corresponding average weight (Figure 4f) of tumor tissues in various groups visually confirmed the efficient growth inhibition by Lip@FePd-DON NPs because it presented the

https://doi.org/10.1021/acsanm.5c02985
ACS Appl. Nano Mater. 2025, 8, 14470−14480

smallest tumor tissue size and lowest tumor tissue weight. As one of the markers for tumor proliferation, a higher positive rate of K_i-67 means a higher growth rate of the tumor.[23] The fluorescence images showed an abundant positive rate of K_i-67 in both the control and Lip groups, which was in agreement with the rapid growth rate of tumor volume (Figure 4g). Obviously decreased K_i-67 was detected in both Lip@FePd and Lip@DON groups compared to the Control group. The Lip@FePd-DON-treated group displayed the lowest level of Ki67, demonstrating that the tumor growth was significantly inhibited. Furthermore, terminal deoxynucleotidyl transferase (TdT)-mediated dUTP nick end labeling (TUNEL) could directly label the apoptotic cells. The strong green fluorescence intensity (Figure 4h) in Lip@FePd, Lip@DON, and Lip@FePd-DON groups confirmed the effective antitumor performance. All of the above results revealed that as-synthesized Lip@FePd-DON NPs could significantly inhibit the growth of breast cancer via ROS-enhanced chemotherapy.

3.5. *In Vivo* Immune Response via Necroptosis-Mediated ICD. Histopathology using hematoxylin and eosin (H&E) staining is a classic and primary diagnostic strategy in cancer treatment.[24] To determine the side effects of Lip@FePd-DON NPs on organs during therapy, histological analyses of vital organs in different treatments were performed. The histological morphology of vital organs, including the heart, liver, spleen, lung, and kidney (Figure S6) presented no obvious abnormalities or necrosis, confirming the good biosafety under the administration dose after i.v. injection. Meanwhile, the H&E staining images of tumor tissues (Figure 5a) clearly showed a high ratio of tumor cells in both control and Lip groups and apparent tumor necroptosis in both Lip@FePd and Lip@FePd-DON groups. This trend was in agreement with the results of immunofluorescence staining (K_i-67 and TUNEL).

As the largest secondary lymphoid organ in the body, the spleen plays an essential role in immune response against pathogens.[25,26] The photographs of the spleen in formulation-treated groups visually showed excess augmentation compared with the Control group (Figure 5b). Meanwhile, the average weight of the Lip@FePd-DON-treated spleen was nearly 2.2-fold bigger than the spleen in the control group (Figure 5c). A previous study has reported that the splenic excess augmentation in tumor-bearing mice was associated with the increased proportion of $CD8^+$ T cells and $CD4^+$ T cells.[27] Thus, we speculated that Lip@FePd-DON-induced necroptosis could effectively trigger an immune response via the release of DAMPs. The tumor tissues were homogenized, and the relevant immune cytokines (TNF-α, IFN-γ, and IL-6) were measured by the ELISA assay. As shown in Figure 5d–f, Lip and Lip@FePd treatment showed no noteworthy change in immune cytokines compared to the control group, revealing that alone, ROS generation could not activate the immune response. In contrast, Lip@DON and Lip@FePd-DON-treated mice presented an obviously upregulated level of TNF-α, IFN-γ, and IL-6 due to the induced necroptosis. Moreover, the tumor in the Lip@FePd-DON group displayed a significantly higher level of IFN-γ than the tumor in the Lip@FePd or Lip@DON group, indicating that both FePd NPs and DON coloaded ROS-generating lipid nanoparticles could make a difference for breast cancer treatment via necroptotic chemo-immunotherapy. In addition, further evaluation of the infiltration and recruitment of $CD8^+$ T cells within the tumor lesions could be done to instigate the systemic antitumor immune response.

4. CONCLUSIONS

In this study, bimetallic FePd NPs and DON coloaded ROS-generating lipid nanoparticles (Lip@FePd-DON NPs) were successfully designed and prepared via the classical thin-film hydration method to enhance necroptotic chemo-immunotherapy for breast cancer. Upon internalization by tumor cells, both bimetallic FePd NPs and DON are released from the lipid NPs via lysosome dissociating. The biocatalytic performance of FePd NPs catalyzes intracellular H_2O_2 to toxic ROS. Meanwhile, the combination of DON and ROS effectively induces cell necroptosis via the RIPK3/MLKL pathway. The therapeutic mechanism was confirmed through cell morphological identification, inhibitor coincubation, immunofluorescence imaging, and western blotting analysis. Furthermore, the immunogenicity of necroptotic cell death releases DAMPs, which act as in situ neoantigens to trigger DCs maturation and T cell activation, resulting in efficient immune response characterized by the expression of inflammatory factors (TNF-α, IFN-γ, and IL-6). Both in vitro and *in vivo* antitumor efficacy demonstrated that the ROS-generating lipid nanoparticles possess significant potential as potential carriers for delivering DON to enhance necroptotic chemo-immunotherapy for breast cancer.

■ ASSOCIATED CONTENT

Supporting Information

The Supporting Information is available free of charge at https://pubs.acs.org/doi/10.1021/acsanm.5c02985.

TEM images of pure Lip (Figure S1), UV–vis–NIR absorption spectra of DON aqueous solution (Figure S2), UV–vis–NIR absorption spectra of H_2O_2/TMB/Lip@FePd-DON mixture with various H_2O_2 concentrations (Figure S3), 4T1 cell viability after coincubation with various concentrations of DON solutions (Figure S4), relative density of protein belt (RIPK3 and GAPDH) calculated by ImageJ software (Figure S5), and H&E images of main organs (heart, liver, spleen, lung, and kidney) in various treatment groups (Figure S6) (PDF)

■ AUTHOR INFORMATION

Corresponding Authors

Lin Wang − *The Department of Oral and Maxillofacial Surgery, Peking University School of Stomatology, Beijing 100081, P. R. China;* orcid.org/0000-0002-0724-2745; Email: linwang@bjmu.edu.cn

Xing Wang − *The State Key Laboratory of Organic–Inorganic Composites, College of Life Science and Technology and The Beijing Laboratory of Biomedical Materials, Beijing University of Chemical Technology, Beijing 100029, P. R. China;* orcid.org/0000-0002-9990-1479; Email: wangxing@mail.buct.edu.cn

Wensheng Xie − *The State Key Laboratory of Organic–Inorganic Composites, College of Life Science and Technology and The Beijing Laboratory of Biomedical Materials, Beijing University of Chemical Technology, Beijing 100029, P. R. China;* orcid.org/0000-0002-1291-3427; Email: derekxws@163.com

https://doi.org/10.1021/acsanm.5c02985
ACS Appl. Nano Mater. 2025, 8, 14470−14480

Authors

Wanting Yang − *The State Key Laboratory of Organic−Inorganic Composites, College of Life Science and Technology and The Beijing Laboratory of Biomedical Materials, Beijing University of Chemical Technology, Beijing 100029, P. R. China*

Ziyao Zhang − *The State Key Laboratory of Organic−Inorganic Composites, College of Life Science and Technology and The Beijing Laboratory of Biomedical Materials, Beijing University of Chemical Technology, Beijing 100029, P. R. China*

Jingxia Xu − *The State Key Laboratory of Organic−Inorganic Composites, College of Life Science and Technology and The Beijing Laboratory of Biomedical Materials, Beijing University of Chemical Technology, Beijing 100029, P. R. China*

Zhuyuan Peng − *The State Key Laboratory of Organic−Inorganic Composites, College of Life Science and Technology and The Beijing Laboratory of Biomedical Materials, Beijing University of Chemical Technology, Beijing 100029, P. R. China*

Fangming Zhang − *The State Key Laboratory of Organic−Inorganic Composites, College of Life Science and Technology and The Beijing Laboratory of Biomedical Materials, Beijing University of Chemical Technology, Beijing 100029, P. R. China*

Xinyu Zhao − *The Key Laboratory of Bioorganic Phosphorus Chemistry & Chemical Biology (Ministry of Education), Department of Chemistry, Tsinghua University, Beijing 100084, P. R. China*

Guofeng Li − *The State Key Laboratory of Organic−Inorganic Composites, College of Life Science and Technology and The Beijing Laboratory of Biomedical Materials, Beijing University of Chemical Technology, Beijing 100029, P. R. China;* orcid.org/0000-0002-4101-0059

Yen Wei − *The Key Laboratory of Bioorganic Phosphorus Chemistry & Chemical Biology (Ministry of Education), Department of Chemistry, Tsinghua University, Beijing 100084, P. R. China*

Lingyun Zhao − *The State Key Laboratory of New Ceramics and Fine Processing, School of Materials 4 Science and Engineering, Tsinghua University, Beijing 100084, P. R. China*

Complete contact information is available at: https://pubs.acs.org/10.1021/acsanm.5c02985

Author Contributions

#W.Y. and Z.Z. have contributed equally to this work. W.Y. performed conceptualization, methodology, and writing−original draft. Z.Z. was in charge of conceptualization, methodology, and writing−original draft. Q.X. performed analysis, review, and editing. Z.P. performed analysis, review, and editing. F.Z. performed analysis, review, and editing. X.Z. performed analysis, review, and editing. G.L. was in charge of methodology, review, and editing. Y.W. was in charge of methodology, review, and editing. L.Z. was in charge of methodology, review, and editing. L.W. was in charge of methodology and writing−review and editing. X.W. performed funding acquisition and writing−review and editing. W.X. was in charge of conceptualization, project administration, funding acquisition, and writing−review and editing.

Notes

The authors declare no competing financial interest.

■ ACKNOWLEDGMENTS

This research was supported by the project of Science and Technology of Yinchuan (2024SFZD004), the Natural Science Foundation of Beijing Municipality (2254093), and the National Natural Science Foundation of China (22275013). Many thanks for the funding support from the Union Project of BUCT-CJFH Biomedical Center (PT2407, 2024-NHLHCRF-YXHZ-MS-05), Union Project of BUCT-PUTH (PT2517), and Fundamental Research Funds for the Central Universities (buctrc202419).

■ REFERENCES

(1) Breast Cancer Expert Committee of National Quality Control Center for Cancer; Breast Cancer Expert Committee of China Anti-Cancer Association; Cancer Drug Clinical Research Committee of China Anti-Cancer Association. Guidelines for Diagnosis and Treatment of Advanced Breast Cancer in China (2022 Edition). *J. Natl. Cancer Cent* **2024**, *4* (2), 107−127.

(2) Schlam, I.; Chavez-MacGregor, M. Best of the Year: Advanced Breast Cancer in 2023. *Breast* **2024**, *74*, No. 103677.

(3) Sonke, G. S.; van Ommen-Nijhof, A.; Wortelboer, N.; van der Noort, V.; Swinkels, A. C. P.; Blommestein, H. M.; Guerrero Paez, C.; Mol, L.; Beeker, A.; Beelen, K.; Hamming, L. C.; Heijns, J. B.; Honkoop, A. H.; de Jong, P. C.; van Rossum-Schornagel, Q. C.; van Schaik-van de Mheen, C.; Tol, J.; Tromp-van Driel, C. S.; Vrijaldenhoven, S.; van Leeuwen-Stok, A. E.; Konings, I. R.; Jager, A.; de Jong, P. C.; van Rossum-Schornagel, Q. C.; van Schaik-van de Mheen, C. Early versus Deferred Use of CDK4/6 Inhibitors in Advanced Breast Cancer. *Nature* **2024**, *636* (8042), 474−480.

(4) Harbeck, N.; Ciruelos, E.; Jerusalem, G.; Müller, V.; Niikura, N.; Viale, G.; Bartsch, R.; Kurzeder, C.; Higgins, M. J.; Connolly, R. M.; Baron-Hay, S.; Gión, M.; Guarneri, V.; Bianchini, G.; Wildiers, H.; Escrivá-de-Romaní, S.; Prahladan, M.; Bridge, H.; Kuptsova-Clarkson, N.; Scotto, N.; Verma, S.; Lin, N. U.; DESTINY-Breast12 study group. Trastuzumab Deruxtecan in HER2-Positive Advanced Breast Cancer with or without Brain Metastases: A Phase 3b/4 Trial. *Nat. Med.* **2024**, 1−11.

(5) Swain, S. M.; Shastry, M.; Hamilton, E. Targeting HER2-Positive Breast Cancer: Advances and Future Directions. *Nat. Rev. Drug Discovery* **2023**, *22* (2), 101−126.

(6) Debien, V.; De Caluwé, A.; Wang, X.; Piccart-Gebhart, M.; Tuohy, V. K.; Romano, E.; Buisseret, L. Immunotherapy in Breast Cancer: An Overview of Current Strategies and Perspectives. *Npj Breast Cancer* **2023**, *9* (1), 1−10.

(7) Galluzzi, L.; Vitale, I.; Warren, S.; Adjemian, S.; Agostinis, P.; Martinez, A. B.; Chan, T. A.; Coukos, G.; Demaria, S.; Deutsch, E.; Draganov, D.; Edelson, R. L.; Formenti, S. C.; Fucikova, J.; Gabriele, L.; Gaipl, U. S.; Gameiro, S. R.; Garg, A. D.; Golden, E.; Han, J.; Harrington, K. J.; Hemminki, A.; Hodge, J. W.; Hossain, D. M. S.; Illidge, T.; Karin, M.; Kaufman, H. L.; Kepp, O.; Kroemer, G.; Lasarte, J. J.; Loi, S.; Lotze, M. T.; Manic, G.; Merghoub, T.; Melcher, A. A.; Mossman, K. L.; Prosper, F.; Rekdal, Ø.; Rescigno, M.; Riganti, C.; Sistigu, A.; Smyth, M. J.; Spisek, R.; Stagg, J.; Strauss, B. E.; Tang, D.; Tatsuno, K.; van Gool, S. W.; Vandenabeele, P.; Yamazaki, T.; Zamarin, D.; Zitvogel, L.; Cesano, A.; Marincola, F. M. Consensus Guidelines for the Definition, Detection and Interpretation of Immunogenic Cell Death. *J. Immunother. Cancer* **2020**, *8* (1), No. e000337.

(8) Galluzzi, L.; Buqué, A.; Kepp, O.; Zitvogel, L.; Kroemer, G. Immunogenic Cell Death in Cancer and Infectious Disease. *Nat. Rev. Immunol.* **2017**, *17* (2), 97−111.

(9) Rucker, A. J.; Park, C. S.; Li, Q. J.; Moseman, E. A.; Chan, F. K.-M. Necroptosis Stimulates Interferon-Mediated Protective Anti-Tumor Immunity. *Cell Death Dis.* **2024**, *15* (6), 1−12.

(10) He, S.; Wang, X. RIP Kinases as Modulators of Inflammation and Immunity. *Nat. Immunol.* **2018**, *19* (9), 912−922.
(11) Lemberg, K. M.; Vornov, J. J.; Rais, R.; Slusher, B. S. We're Not "DON" Yet: Optimal Dosing and Prodrug Delivery of 6-Diazo-5-Oxo-L-Norleucine. *Mol. Cancer Ther.* **2018**, *17* (9), 1824−1832.
(12) Rahman, A.; Smith, F. P.; Luc, P. T.; Woolley, P. V. Phase I Study and Clinical Pharmacology of 6-Diazo-5-Oxo-L-Norleucine (DON). *Invest. New Drugs* **1985**, *3* (4), 369−374.
(13) Hensley, C. T.; Wasti, A. T.; DeBerardinis, R. J. Glutamine and Cancer: Cell Biology, Physiology, and Clinical Opportunities. *J. Clin. Invest.* **2013**, *123* (9), 3678−3684.
(14) Tenora, L.; Alt, J.; Dash, R. P.; Gadiano, A. J.; Novotná, K.; Veeravalli, V.; Lam, J.; Kirkpatrick, Q. R.; Lemberg, K. M.; Majer, P.; Rais, R.; Slusher, B. S. Tumor-Targeted Delivery of 6-Diazo-5-Oxo-l-Norleucine (DON) Using Substituted Acetylated Lysine Prodrugs. *J. Med. Chem.* **2019**, *62* (7), 3524−3538.
(15) Rais, R.; Jančařík, A.; Tenora, L.; Nedelcovych, M.; Alt, J.; Englert, J.; Rojas, C.; Le, A.; Elgogary, A.; Tan, J.; Monincová, L.; Pate, K.; Adams, R.; Ferraris, D.; Powell, J.; Majer, P.; Slusher, B. S. Discovery of 6-Diazo-5-Oxo-l-Norleucine (DON) Prodrugs with Enhanced CSF Delivery in Monkeys: A Potential Treatment for Glioblastoma. *J. Med. Chem.* **2016**, *59* (18), 8621−8633.
(16) Rais, R.; Lemberg, K. M.; Tenora, L.; Arwood, M. L.; Pal, A.; Alt, J.; Wu, Y.; Lam, J.; Aguilar, J. M. H.; Zhao, L.; Peters, D. E.; Tallon, C.; Pandey, R.; Thomas, A. G.; Dash, R. P.; Seiwert, T.; Majer, P.; Leone, R. D.; Powell, J. D.; Slusher, B. S. Discovery of DRP-104, a Tumor-Targeted Metabolic Inhibitor Prodrug. *Sci. Adv.* **2022**, *8* (46), No. eabq5925.
(17) Tenchov, R.; Bird, R.; Curtze, A. E.; Zhou, Q. Lipid Nanoparticles—From Liposomes to mRNA Vaccine Delivery, a Landscape of Research Diversity and Advancement. *ACS Nano* **2021**, *15* (11), 16982−17015.
(18) Xie, W.; Li, Y.; Guo, Z.; Lu, J.; Li, G.; Zhang, Z.; Zhang, F.; Wei, Y.; Wang, X.; Zhao, L. FePd Nanozyme- and SKN-Encapsulated Functional Lipid Nanoparticles for Cancer Nanotherapy via ROS-Boosting Necroptosis. *ACS Appl. Mater. Interfaces* **2024**, *16* (15), 18411−18421.
(19) Xie, W.; Zhang, G.; Guo, Z.; Lu, J.; Ye, J.; Xu, W.; Gao, X.; Yue, K.; Wei, Y.; Zhao, L. Ultra-Sensitive Iron-Doped Palladium Nanocrystals with Enhanced Hydroxyl Radical Generation for Chemo-/Chemodynamic Nanotherapy. *Adv. Funct. Mater.* **2022**, *32* (12), No. 2107518.
(20) Ziegler, U.; Groscurth, P. Morphological Features of Cell Death. *Physiology* **2004**, *19* (3), 124−128.
(21) Zhang, Z.; Zhang, F.; Xie, W.; Niu, Y.; Wang, H.; Li, G.; Zhao, L.; Wang, X.; Xie, W. Induced Necroptosis and Its Role in Cancer Immunotherapy. *Int. J. Mol. Sci.* **2024**, *25* (19), No. 10760.
(22) Liu, S.; Perez, P.; Sun, X.; Chen, K.; Fatirkhorani, R.; Mammadova, J.; Wang, Z. MLKL Polymerization-Induced Lysosomal Membrane Permeabilization Promotes Necroptosis. *Cell Death Differ.* **2024**, *31* (1), 40−52.
(23) Uxa, S.; Castillo-Binder, P.; Kohler, R.; Stangner, K.; Müller, G. A.; Engeland, K. Ki-67 Gene Expression. *Cell Death Differ.* **2021**, *28* (12), 3357−3370.
(24) Lin, J.-R.; Chen, Y.-A.; Campton, D.; Cooper, J.; Coy, S.; Yapp, C.; Tefft, J. B.; McCarty, E.; Ligon, K. L.; Rodig, S. J.; Reese, S.; George, T.; Santagata, S.; Sorger, P. K. High-Plex Immunofluorescence Imaging and Traditional Histology of the Same Tissue Section for Discovering Image-Based Biomarkers. *Nat. Cancer* **2023**, *4* (7), 1036−1052.
(25) Bronte, V.; Pittet, M. J. The Spleen in Local and Systemic Regulation of Immunity. *Immunity* **2013**, *39* (5), 806−818.
(26) Lewis, S. M.; Williams, A.; Eisenbarth, S. C. Structure and Function of the Immune System in the Spleen. *Sci. Immunol.* **2019**, *4* (33), No. eaau6085.
(27) Hui, D.; Guoqiang, Z.; Anguo, T.; Qianyun, Z.; Jing, C.; Jingjing, F.; Anjun, L. Mechanism of Splenic Excess Augmentation in Tumor-bearing Mice. *Cancer Res. Prev. Treat.* **2012**, *39* (8), 940−943.

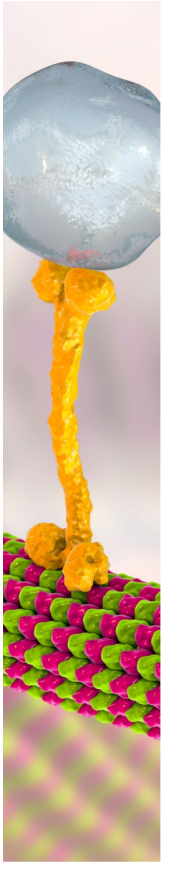

https://doi.org/10.1021/acsanm.5c02985
ACS Appl. Nano Mater. 2025, 8, 14470−14480